Acquisition of cell migration defines NK cell differentiation from hematopoietic stem cell precursors

Barclay J. Lee[a,b] and Emily M. Mace[b,c,*]
[a]Department of Bioengineering, Rice University, Houston, TX 77005; [b]Center for Human Immunobiology, Texas Children's Hospital, Houston, TX 77030; [c]Department of Pediatrics, Baylor College of Medicine, Houston, TX 77030

ABSTRACT **Human natural killer (NK) cells are generated from CD34$^+$ precursors and can be differentiated in vitro by coculture with developmentally supportive stromal cells. We have previously described the acquisition of cell migration as a feature of NK cell terminal maturation in this system. Here we perform continuous long-term imaging and tracking of NK cell progenitors undergoing in vitro differentiation. We demonstrate that NK cell precursors can be tracked over long time periods on the order of weeks by utilizing phase-contrast microscopy and show that these cells acquire increasing motility as they mature. Additionally, we observe that NK cells display a more heterogeneous range of migratory behaviors at later stages of development, with the acquisition of complex modes of migration that are associated with terminal maturation. Together these data demonstrate previously unknown migratory behaviors of innate lymphocytes undergoing lineage differentiation revealed by long-term imaging and analysis workflows.**

Monitoring Editor
Carole Parent
University of Michigan

Received: Aug 14, 2017
Revised: Sep 27, 2017
Accepted: Oct 3, 2017

INTRODUCTION

Human natural killer (NK) cells are derived from CD34$^+$ hematopoietic stem cell precursors that originate in the bone marrow and undergo terminal maturation in secondary lymphoid tissue (Freud *et al.*, 2005; Eissens *et al.*, 2012). Their differentiation has been stratified to five stages, with each stage marked by differential expression of surface markers, production of cytokines, and ability to perform cytotoxic functions (Freud *et al.*, 2005, 2006). Although originally these stages were identified in secondary lymphoid and tonsillar tissue, it is now appreciated that NK cells can likely undergo maturation in a variety of microenvironments within the body (Eissens *et al.*, 2012; Yu *et al.*, 2013). This has led to a model in which early NK cell precursors seed peripheral tissue and give rise to mature NK cells before entering circulation.

Within peripheral blood, NK cells are found within the distinct functional and phenotypic subsets termed CD56^{bright} or CD56^{dim}. These subsets are thought to represent discrete stages of the model described above, with multiple lines of evidence suggesting that the CD56^{bright} (stage 4) subset is a direct precursor of terminally differentiated CD56^{dim} (stage 5) NK cells (Chan *et al.*, 2007; Huntington *et al.*, 2009; Eissens *et al.*, 2012). However, given the seeming plasticity in environments that can support NK cell development, as well as the poor correlation between human and murine NK cell phenotypes, human NK cell differentiation is a poorly understood process. Human NK cell development can be studied with an in vitro model, which is also of interest for the generation of clinical-grade NK cells for immune therapy (Dezell *et al.*, 2012; Rezvani and Rouce, 2015). The most efficient method for in vitro differentiation of human NK cells from CD34$^+$ progenitor cells is through coculture with an irradiated feeder layer of stromal cells, specifically the EL08.1D2 cell line (Grzywacz *et al.*, 2006; Dezell *et al.*, 2012). CD34$^+$ cell culture under these conditions leads to high commitment to the NK cell lineage, with 99% purity after 35 d of culture described (Grzywacz *et al.*, 2006). In vitro–derived NK cells have cytotoxic function and exhibit many of the same surface markers observed on mature NK cells derived from patient blood (Miller and McCullar, 2001; Grzywacz *et al.*, 2006; Eissens *et al.*, 2012). NK cells can also be derived from progenitor cells in the presence of cytokines alone,

This article was published online ahead of print in MBoC in Press (http://www.molbiolcell.org/cgi/doi/10.1091/mbc.E17-08-0508) on October 11, 2017.

*Address correspondence to: Emily Mace (mace@bcm.edu).

Abbreviations used: HSC, hematopoietic stem cell; MSD, mean squared displacement; NKDI, NK cell developmental intermediate.

but allowing contact with developmentally supportive stromal cells significantly increases cell proliferation as well as maturation (Miller and McCullar, 2001; Grzywacz *et al.*, 2006).

Despite the requirement for direct stromal cell contact in this system, the intercellular interactions between the $CD34^+$ progenitors and the EL08.1D2 cells driving this developmental pathway are as of yet unclear and deserve further study. Incubation of $CD56^{bright}$ or $CD56^{dim}$ NK cells on EL08.1D2 stroma leads to significant nondirected migration on stromal cells. Furthermore, isolation of NK cell developmental intermediates (NKDI) from tonsillar tissue or in vitro differentiation identifies distinct migratory behavior based on developmental stage (Mace *et al.*, 2016). Progression through differentiation is associated with increased velocity of migrating cells and decreased time spent in arrest. These migratory properties are conserved in both NKDI isolated from tonsillar tissue and NK cells generated in vitro from $CD34^+$ precursors (Mace *et al.*, 2016).

With current microscopy technology, it is now feasible to perform long-term time-lapse imaging of cells with sufficient time resolution to adequately track cell movements. Many modern microscope systems allow for temperature and environmental regulation to ensure cell stability over a long period of time. Thus a growing challenge in the field is how to best acquire and process large amounts of migration data in the most efficient and accurate manner. Typically, tracking is performed on cells labeled with a fluorescent dye, but this method is unsuited for long-term imaging, where phototoxicity and dye loss become problems (Coutu and Schroeder, 2013). Transmitted light microscopy avoids this issue but makes tracking cells more difficult due to the lower signal-to-noise ratio in these images. In this case, tracking is often done manually, which is extremely time-consuming and allows for user bias. Reliable automated methods for tracking transmitted light images are thus highly desirable but currently lacking, although improvements have been made in recent years (Hilsenbeck *et al.*, 2016; Xing and Yang, 2016).

In this study, we show, for the first time, the continuous development of human NK cells from $CD34^+$ hematopoietic stem cells (HSC) and demonstrate that the acquisition of motility is progressively acquired through NK cell maturation. We further quantify the heterogeneity in the developing NK cell migration phenotype by classifying single-cell tracks by their speed and mode of migration (directed, constrained, or random). Together these results define the acquisition of human NK cell migratory capacity throughout development using high temporal resolution and continuous length of imaging.

RESULTS AND DISCUSSION

Human NK cell types exhibit distinct migratory behavior on stromal cells

NK cell lines and ex vivo NK cells undergo migration on EL08.1D2 stromal cells when assayed over relatively short periods of imaging (Mace *et al.*, 2016). To compare their migratory behavior and validate the sensitivity of our long-term imaging system, we labeled NK92 and YTS cell lines and ex vivo NK cells (eNK) with CellTracker Violet dye and cocultured them with EL08.1D2 cells for 24 h. The cells were continuously imaged at 2-min intervals, and following acquisition the cells were tracked in Imaris following segmentation based on fluorescence (Figure 1A). eNK and NK cell lines had distinct migratory properties classified by mean speed, straightness, and arrest coefficient. eNK cells had more directed motion overall, characterized by significantly higher track straightness and lower arrest coefficient (frequency of time that cells were in arrest) than both cell lines (Figure 1, B and C). There were significant differences in motility between the two NK cell lines, with NK92 cells having higher overall speeds than YTS cells and lower arrest coefficients, although straightness was not significantly different (Figure 1, B and C). This experiment validated that we were able to accurately track cell movements and revealed interesting variations between NK cell types in terms of motility. This is in agreement with previous reports of NK92 and YT cells (from which the YTS line is derived) showing differential migration within Matrigel (Edsparr *et al.*, 2009).

NK cell precursor motility and phenotype changes throughout maturation

As eNK cells show significant motility on stromal cells, and acquisition of migratory behavior is associated with NK cell development in vitro and in vivo (Mace *et al.*, 2016), we sought to define the migratory behavior of NK cell precursors throughout development. Specifically, we aimed to measure cell migratory properties with minimally invasive imaging in a large field of view in order to not bias analyses with cells that may leave the imaging field. Using our long-term imaging system described above, we generated human NK cells in vitro from purified $CD34^+$ HSC cocultured on a developmentally supportive monolayer of EL08.1D2 stromal cells (Grzywacz *et al.*, 2006; Mace *et al.*, 2016). Cells were imaged continuously every 2 min throughout the 21-d period required for maturation into NK cells. As expected, some stromal cell death was observed at later time points, but nevertheless NKDI continued to migrate and differentiate (Figure 2A). While untested in the current study, we hypothesize that the deposition of extracellular matrix proteins by stromal cells may contribute to the retained ability of NKDI to migrate on surfaces upon which stromal cells have previously been cultured. Individual cells were segmented and tracked for parameters including track speed, length, and displacement to measure how their migratory behaviors evolved throughout differentiation (Figure 2A). All tracking was done on phase-contrast images because we found that fluorescent cellular dyes did not persist throughout the entire 4-wk period. Using this method enabled the tracking of single cells for extended periods of imaging (Supplemental Movie 1).

To quantify the migratory behavior of developing NK cells early in differentiation, tracks were extracted from continuous 24-h periods at days 0, 7, 14, and 21. Although not all tracks were continuous throughout the time of imaging, mean speed and displacement increased significantly at each progressive time point (Figure 2B), and visual inspection confirmed that average cell track length increased significantly throughout the time of differentiation (Figure 2B and Supplemental Movies 2 and 3).

Initially, $CD34^+$ cells had minimal speed (0.85 ± 0.20 μm/min), track length (273.6 ± 107.9 μm), and displacement (19.68 ± 11.98 μm) over the initial 24-h period. However, at day 21, mean speed was 1.48 ± 0.48 μm/min, consistent with previously reported migration speeds of mature NK cells (Khorshidi *et al.*, 2011; Mace *et al.*, 2016). Path length increased over time as well but was significant only between the 7- and 14-d time points (Figure 2B). Given the significant differences between days 0 and 14, we performed an additional experimental replicate where cells were tracked for consecutive 24-h movies over the first 14 d of imaging. Significant variations in mean speed, displacement, and path length were observed between daily time points, which cumulatively accounted for the overall trends previously described at the weekly time points (Figure 2C). On the basis of these results, we concluded that the acquisition of track speed and length in developing NK cells occurs progressively throughout the initial stages of differentiation. A similar increase in speed has been similarly described in developing human T-cells, as relatively immature (double-negative and double-positive)

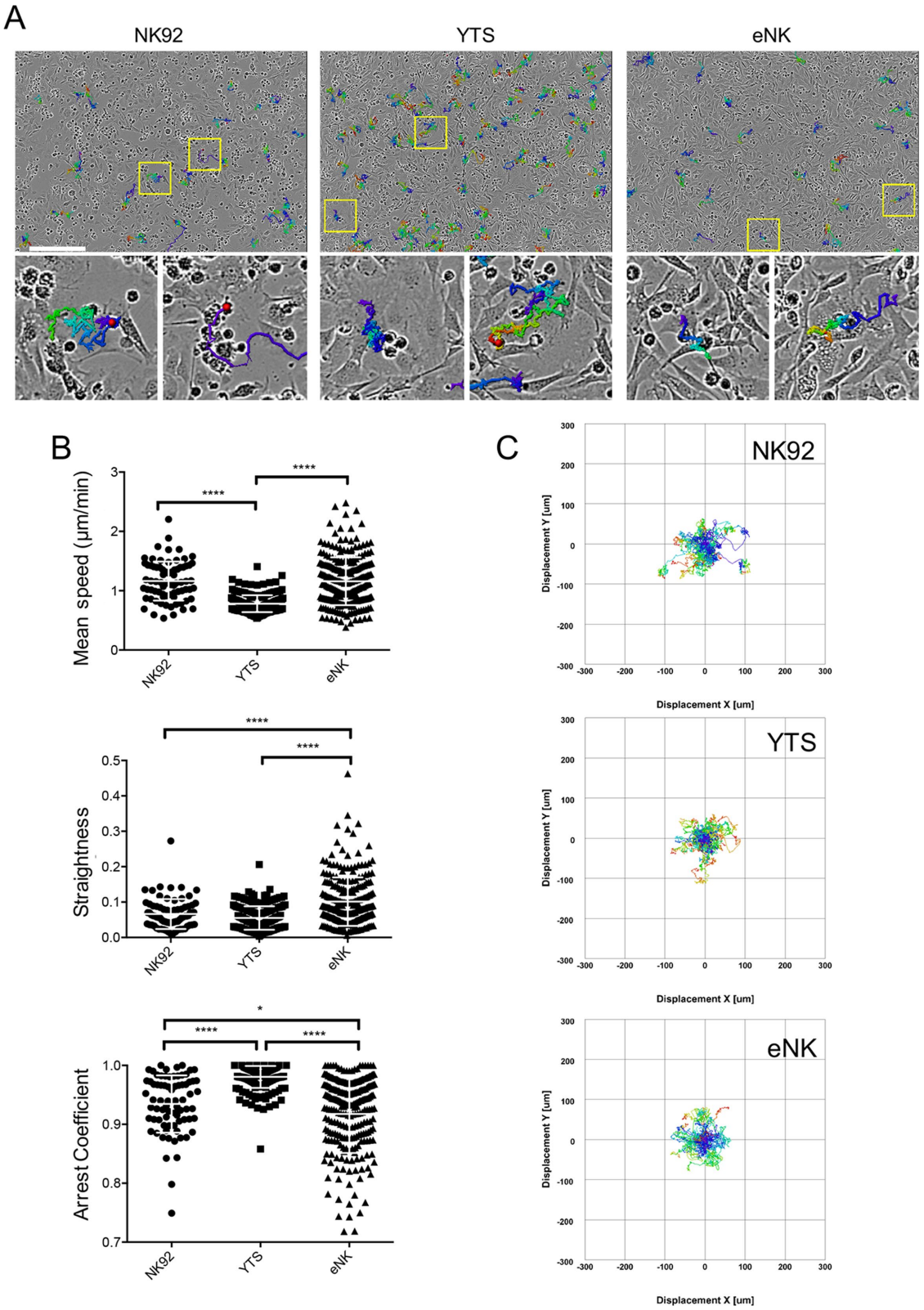

FIGURE 1: Continuous live-cell imaging of human NK cells on stromal cells. YTS or NK92 NK cell lines or human NK cells (eNK) were labeled with CellTracker Violet and then cocultured with an irradiated EL08.1D2 monolayer for 24 h in a 96-well plate. Images were acquired continuously every 2 min. (A) Representative phase-contrast images of each cell type with randomly selected sample tracks overlaid. Insets show zoomed-in views of single-cell tracks. Scale bar = 300 µm. (B) Mean track speed (top), straightness (center), and arrest coefficient (bottom) of NK cells were calculated. Error bars indicate SD. Means with significant differences were determined by ordinary one-way ANOVA with Tukey's multiple comparison test; *$p < 0.05$, ****$p < 0.0001$). Data are representative of three independent experiments. $n = 75$ (NK92), 205 (YTS), and 250 (eNK). (C) Rose plots of representative tracks. $n = 30$ per graph.

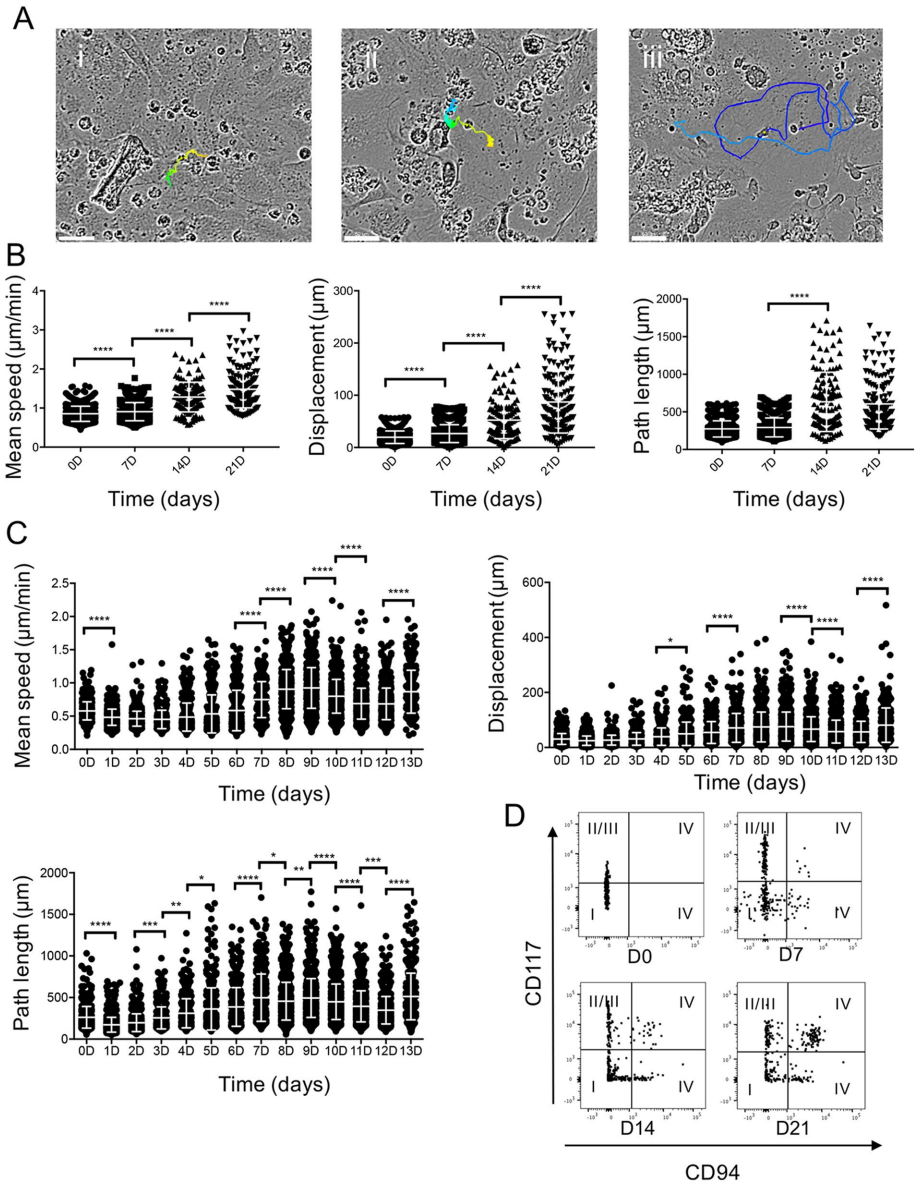

FIGURE 2: Acquisition of intrinsic NK cell migration with differentiation. CD34⁺ HSCs were seeded on a monolayer of EL08.1D2 cells. Cells were imaged continuously in phase-contrast mode for 21 d. Images were acquired every 2 min, and tracking was done over a 24-h period for each time point. FACS analysis was performed weekly to monitor expression of developmental markers. (A) Representative images of NK cell intermediates with randomly selected tracks 0 (i), 7 (ii), and 21 (iii) d after the start of the experiment. Scale bar = 50 μm. (B) Mean speed, displacement, and path length of NK cell developmental intermediates were measured at 7-d intervals as indicated. Error bars indicate SD. ****$p < 0.0001$ by ordinary one-way ANOVA with Tukey's multiple comparisons test. $n = 932$ (0D), 803 (7D), 134 (14D), and 148 (21D). (C) Mean speed, displacement, and path length of cells from continuous tracking from the first 14 d are shown as 24 h segments. Error bars indicate SD. Means with significant differences as analyzed by ordinary one-way ANOVA with Tukey's multiple comparison test are shown (*$p < 0.05$, **$p < 0.01$, ***$p < 0.001$, ****$p < 0.0001$). Sample sizes for each individual time point are listed in *Materials and Methods*. (D) FACS analysis of NK cell maturation markers. Predicted NK cell developmental stage based on phenotype as described in the text is shown in Roman numerals. All data shown are representative of three independent experiments.

thymocytes have substantially slower track speeds than their more mature single-positive counterparts (Ehrlich *et al.*, 2009; Halkias *et al.*, 2013). On average, observed progenitor cell speeds at all stages were similar to those measured for immortalized NK cell lines as well as those seen in other studies looking at lymphocyte motility, both in vitro (Khorshidi *et al.*, 2011; Zhou *et al.*, 2017) and in vivo (Miller *et al.*, 2002; Ehrlich *et al.*, 2009).

Progression of NK cell development was additionally monitored by flow cytometry analysis of NK cell developmental markers at days 0, 7, 14, and 21. We analyzed cells for expression of CD117 and CD94, which, when considered with CD34, identify developmental stages 1–4, and CD16, a marker of NK cell terminal maturation (Freud *et al.*, 2006; Eissens *et al.*, 2012). NK cells undergo differentiation through four linear stages: stage 1 cells are $CD34^+CD117^-CD94^-$, stage 2 cells are $CD34^+CD117^+CD94^-$, stage 3 cells are $CD34^-CD117^+CD94^-$, and stage 4 cells are $CD34^-CD117^{+/-}CD94^+$. Following lymphocyte gating on forward and side scatter to define the NKDI population (Supplemental Figure 1A), we observed that increasing frequencies of cells underwent differentiation to stage 4 (27% at day 21), which was accompanied by a decreasing frequency of immature cells at later time points (Figure 2D).

NK cell developmental intermediates in later stages of development exhibit more directed migration

Given the increasing speed and track length associated with migration of developing NK cells, we sought to further quantify the degree of directed migration in NK cell tracks by calculating the straightness and arrest coefficients. This was performed first on tracks extracted from 7-d intervals (Figure 3A). An increase in straightness and a decrease in arrest coefficient over time were observed for the weekly time points (Figure 3A). While $CD34^+$ HSC (0D) had a track straightness of 0.074 ± 0.05, at the 21D time point, the mean straightness index was 0.149 ± 0.10. Similarly, the arrest coefficient decreased from 0.993 ± 0.01 to 0.884 ± 0.1 between the 0- and 21-d time points. This was in agreement with the increase in mean speed observed for the later time points. As demonstrated for the significant changes in track speed between days 14 and 21, straightness and arrest coefficient similarly had the greatest changes in this time interval (Figure 3A). Although significant differences from day to day were detected, the overall change in these statistics is relatively small compared with those observed between days 0 and 21 (Figure 3, A and B).

Mode of migration depends on NK cell developmental stage

Migrating cells can exhibit either directed motion, constrained motion, or random diffusion (Krummel *et al.*, 2016). Random diffusion represents the type of movement expected of a cell of a certain size

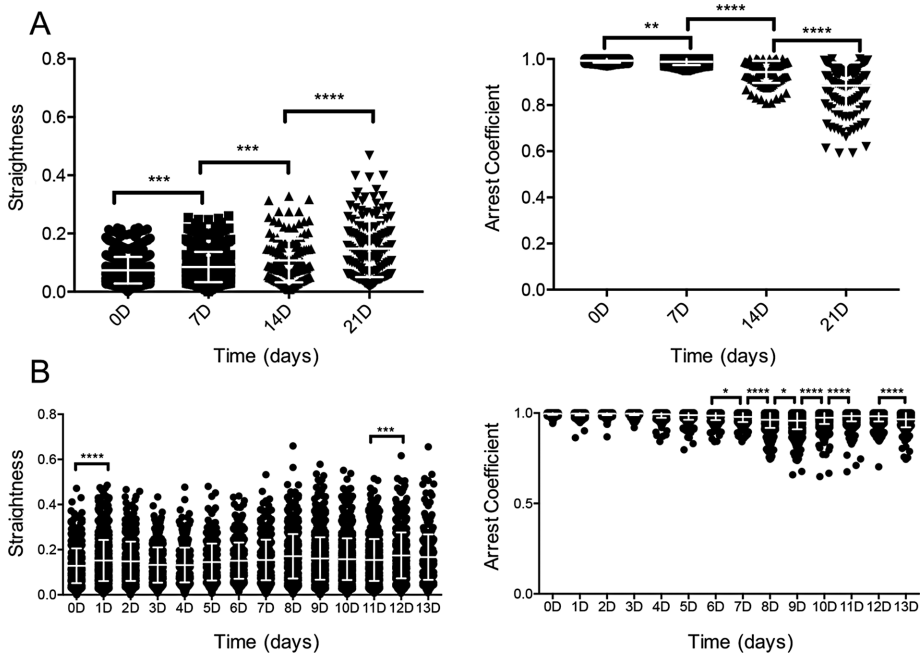

FIGURE 3: NK cell differentiation leads to increasingly directed migration. (A) Straightness and arrest coefficient for NK cell tracks at weekly time points. Error bars indicate SD. Means with significant differences as analyzed by ordinary one-way ANOVA with Tukey's multiple comparison test are shown (**$p < 0.01$, ***$p < 0.001$, ****$p < 0.0001$). $n = 932$ (0D), 803 (7D), 134 (14D), and 148 (21D). (B) Straightness and arrest coefficient for NK cell tracks at daily time points. Error bars indicate SD. Means with significant differences are determined by ordinary one-way ANOVA with Tukey's multiple comparison test (*$p < 0.05$, ***$p < 0.001$, ****$p < 0.0001$). Sample sizes for each individual time point are listed in *Materials and Methods*. All data shown are representative of three independent experiments.

due to Brownian motion (Khorshidi *et al.*, 2011). In this case, the mean square displacement (MSD) will be linear with time, whereas directed or constrained tracks will deviate above or below the linear trend, respectively (Krummel *et al.*, 2016). To characterize the diffusivity of our NK cell precursors, we calculated the MSD of NK cell tracks at the weekly time points (Figure 4A). In agreement with our previous measurements of track length and displacement, MSD progressively increased over time, starting at 546.8 ± 549.6 μm^2 at day 0 for $t = 450$ min and increasing to 6405.0 ± 10,447.7 μm^2 at day 21 for the same t value.

While these values reflected a population-based measurement, many cells exhibited complex behaviors with multiple modes contained within a single track. To classify cell tracks by their transient properties, we implemented a previously described method for analyzing NK cell migration (Khorshidi *et al.*, 2011). Using this method for each track, we calculated both the diffusion coefficient D and the diffusion exponent α, which define the slope and curvature of the MSD curve, respectively. Tracks were classified by mode of migration by thresholding on these values (Figure 4B). Applying this analysis to all tracks for a given time point gave the fraction of time cells spent in either constrained or directed migration. At day 0, 99.2% of cells exhibit purely constrained motion and 0% of cells exhibit purely directed motion (Figure 4C). This had changed significantly by day 21, with 39.2% of cells exhibiting purely constrained tracks and 3.4% of cells exhibiting purely directed motion (Figure 4D). These results suggest that the increase in mean speed over developmental stage that was described previously is due to a greater propensity for more mature cells to undergo directed migration. By analyzing the MSD of cell tracks, we observed significantly more directed walks at later stages of NK cell differentiation. This could reflect a migration strategy adopted by more functional NK cell intermediates to maximize target cell killing.

Many cells measured at later time points exhibited seemingly Lévy-type walks, characterized by periods of extended cell arrest interspersed with short, highly directional movements. We propose that this arrest results from direct cell contact with the surrounding stromal or extracellular matrix (ECM) microenvironment. $CD8^+$ T-cells similarly utilize Lévy walks, with computational modeling suggesting that this behavior increases the efficiency of locating target cells compared with a purely random walk (Harris *et al.*, 2012). Inhibiting T-cell turning, such as through deletion of the nonmuscle myosin motor myosin 1g, leads to decreased detection of rare antigens and supports the idea that an inability to effectively perform Lévy-type walks results in a less efficient search strategy (Gerard *et al.*, 2014). In NK cells, similar transient periods of arrest have been previously described to correspond to the formation of conjugates with target cells and cell-mediated killing, although they can also occur spontaneously (Khorshidi *et al.*, 2011). Interestingly, IL-2–activated NK cells, which have greater cytolytic activity than unstimulated cells, spend much less time in arrest while also forming twice as many cell contacts compared with resting NK cells (Olofsson *et al.*, 2014). Similarly, NK cell licensing leads to longer-lived and more effective NK-target conjugates, suggesting that regulation of conjugate formulation and migration behavior correlates with relevant functional differences, such as cytotoxic capacity (Forslund *et al.*, 2015). Therefore the acquisition of this specific mode of migration may represent a previously unappreciated component of functional maturation. Alternatively, the seeking behavior that develops may enable the location of key developmental cues that are required for NKDI to proceed through differentiation. It will be of interest to determine whether this behavior is a requirement for, or a product of, NK cell maturation.

NK cell maturation is accompanied by increased heterogeneity in NK cell migratory behavior

While we observed a global increase in cell motility over time, we also observed increasing heterogeneity of cell migratory behaviors with progressive NK cell maturation. This heterogeneity is likely due, in part, to the phenotypic heterogeneity defined by our flow cytometry data. To define heterogeneity within single-cell tracks, we calculated the number of alternations between different migration modes that occurred for each track. Plotting the distribution for migration mode switching at each weekly time point, we observed a progressive increase in the number of alternations over time (Figure 5A). However, later time points still retained a subset of tracks that underwent very few alternations. As a separate measure of migratory heterogeneity, we also calculated the SD of the intraframe speeds observed for each track, as a larger SD would be indicative of a track with a greater variation in migratory modes. An increased SD of track speeds at later time points was seen when we measured track

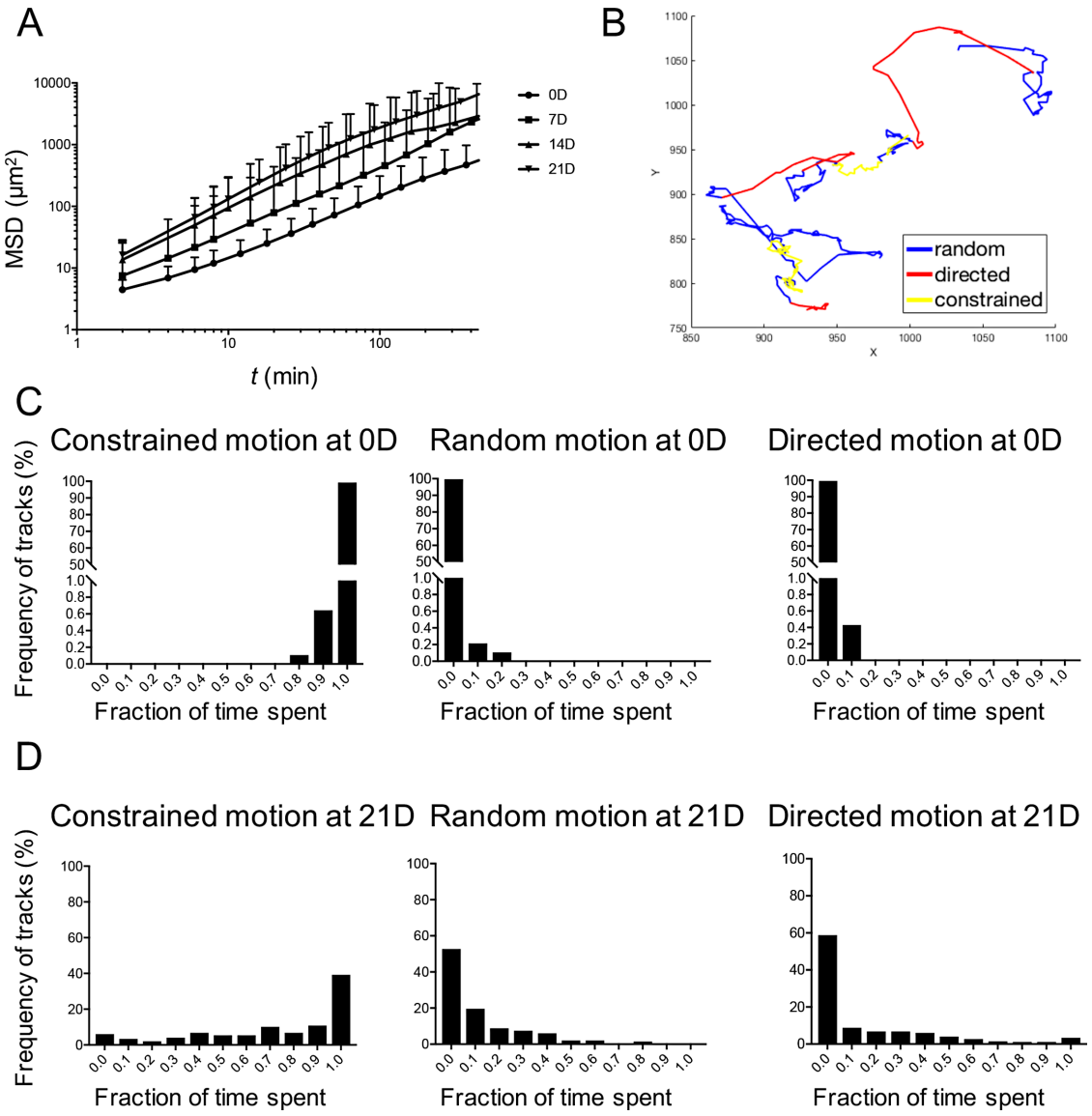

FIGURE 4: NK cell differentiation is associated with distinct modes of migration. (A) MSD of tracks acquired at weekly time points. Graph is truncated at 450 min because few cell tracks persist for longer. Error bars indicate SD. (B) Representative NK cell track after 21 d of development shown with segments corresponding to each migration mode labeled. (C) Fraction of time spent in either constrained, random, or directed motion for each cell after 0 d of development. $n = 932$. (D) Fraction of time spent in either constrained, random, or directed motion for each cell after 21 d of development. $n = 148$. All data shown are representative of three independent experiments.

statistics from both the weekly and consecutive daily data sets (Figure 5B). The mean SD increased from 0.39 ± 0.11 μm/min at day 0 to 1.07 ± 0.51 μm/min by day 21. However, this heterogeneity was also due to the shift toward complex behaviors defined by the measurement of heterogeneity within single-cell tracks. At the beginning of tracking, cells exhibited primarily low-speed constrained tracks, whereas at later times there was a greater frequency of behaviors such as tracks resembling Lévy-type superdiffusive walks, characterized by a series of short, constrained motions interspersed with periods of highly directed motion (Harris *et al.*, 2012; Krummel *et al.*, 2016). Additionally, a small subset of mature cells exhibited purely ballistic migration, traveling in essentially a straight line for the duration of migration, particularly at later time points (Figure 4D).

Conclusion

In summary, we have shown that NK cells acquire motility throughout development, progressing from a mostly constrained migratory phenotype to complex walks and more directed migration. The transition to this mode of migration strategy may enable more efficient target cell killing by increasing the rate at which NK cells can conjugate with targets. Additionally, the increased heterogeneity in cell migration at later stages may correspond to NK cells with different functional capabilities, with cells exhibiting greater motility being more effective at cell-mediated cytotoxicity (Choi and Mitchison, 2013; Forslund *et al.*, 2015; Zhou *et al.*, 2017). Continuing to study NK cell dynamics at the single-cell level will likely lead to greater understanding of their development and function.

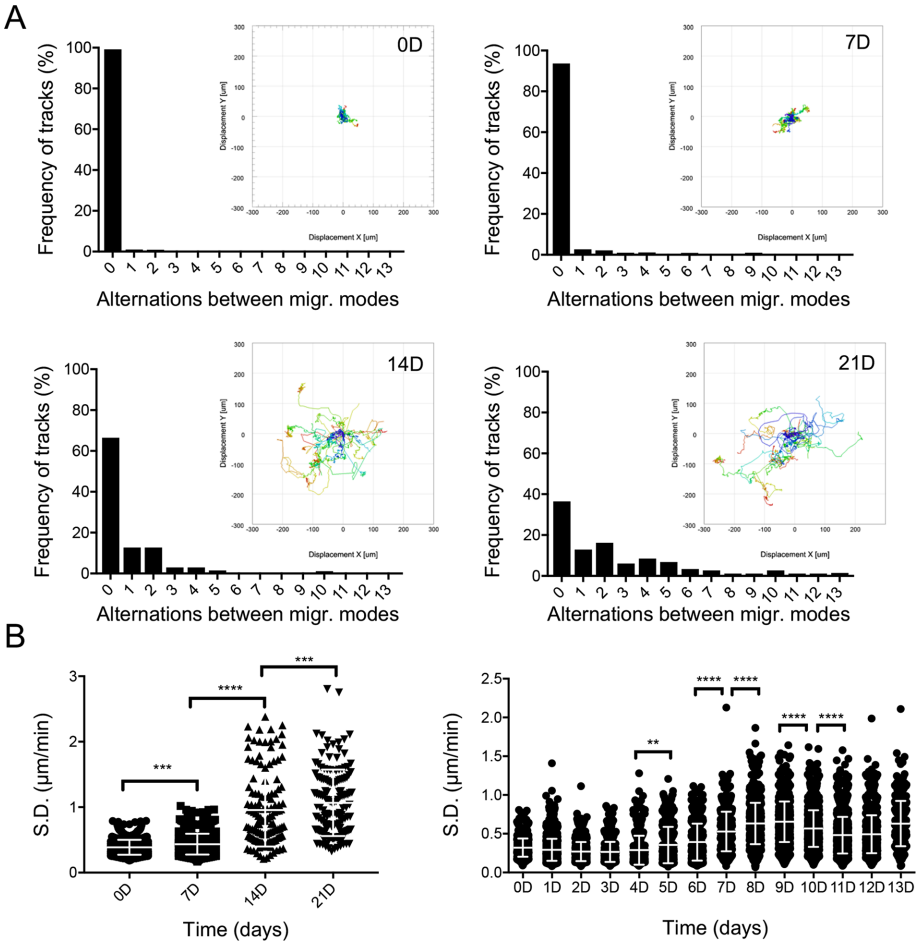

FIGURE 5: NK cell maturation is correlated with increased heterogeneity of migratory phenotype. (A) Number of alternations between migration modes for cell tracks observed at the weekly time points. $n = 932$ (0D), 803 (7D), 134 (14D), 148 (21D). Insets: Rose plots of representative tracks. $n = 20$ per graph. (B) SD of the instantaneous speeds observed for each track for daily time points and weekly time points. Error bars indicate SD. Significance between means determined by ordinary one-way ANOVA with Tukey's multiple comparisons test: $^{**}p < 0.01$, $^{***}p < 0.001$, $^{****}p < 0.0001$. $n = 932$ (0D), 803 (7D), 134 (14D), and 148 (21D). All data shown are representative of three independent experiments.

MATERIALS AND METHODS

Cell culture

EL08.1D2 cells stromal cells (a gift from J. Miller, University of Minnesota) were maintained on gelatinized culture flasks at 32°C in 40.5% α-MEM (Life Technologies), 50% Myelocult M5300 (STEMCELL Technologies), 7.5% heat-inactivated fetal calf serum (FCS; Atlanta Biologicals) with β-mercaptoethanol (10^{-5} M), Glutamax (Life Technologies; 2 mM), penicillin/streptomycin (Life Technologies; 100 U ml^{-1}), and hydrocortisone (Sigma, 10^{-6} M). Culture media was supplemented with 20% conditioned supernatant from previous EL08.1D2 cultures.

Before stromal cell seeding for in vitro $CD34^+$ differentiation, 96-well plates were treated with 0.1% gelatin in ultrapure water to promote cell adherence. Fifty microliters of 0.1% gelatin was deposited on 96-well plates and incubated at room temperature for 10 min. Following incubation, wells were washed with phosphate-buffered saline (PBS) and left for an additional 60 min in a sterile culture hood to dry. Gelatinized 96-well plates were seeded with a confluent layer of EL08.1D2 cells at a density of (5–10) × 10^3 cells per well and then mitotically inactivated by irradiation at 300 rad. Purified $CD34^+$ hematopoietic stem cells were cultured at a density of (2–20) × 10^3 cells per well on these EL08.1D2-coated plates in Ham's F12 media (Corning) plus DMEM (Life Technologies; 1:2) with 20% human AB^- serum (Atlanta Biologicals), ethanolamine (Sigma Aldrich; 50 µM), ascorbic acid (Sigma Aldrich; 20 mg l^{-1}), sodium selenite (Sigma Aldrich; 5 µg l^{-1}), β-mercaptoethanol (Life Technologies; 24 µM), and penicillin/streptomycin (Life Technologies; 100 U ml^{-1}) in the presence of IL-15 (5 ng ml^{-1}), IL-3 (5 ng ml^{-1}), IL-7 (20 ng ml^{-1}), Stem Cell Factor (20 ng ml^{-1}), and Flt3L (10 ng ml^{-1}) (all cytokines from Peprotech). Half-media changes were performed every 7 d, excluding IL-3 after the first week.

NK92 cells (American Type Culture Collection) were maintained in Myelocult H5100 (STEMCELL Technologies) with IL-2 (200 U ml^{-1}). YTS cells (a gift from J. Strominger, Harvard University) were maintained in RPMI 1640 (Life Technologies), 10% FCS (Atlanta Biologicals), HEPES (Life Technologies; 10 µM), penicillin/streptomycin (Life Technologies; 100 U ml^{-1}), MEM Non-Essential Amino Acids Solution (Thermo Fisher; 1 mM), sodium pyruvate (1 mM), and L-glutamine (2 mM). All cell lines were authenticated by flow cytometry and confirmed monthly to be mycoplasma free.

$CD34^+$ precursor isolation and flow cytometry

T- and B-cell lineage depletion was performed using NK cell RosetteSep enrichment (STEMCELL Technologies) and Ficoll-Paque density gradient centrifugation from routine red cell exchange apheresis performed at Texas Children's Hospital. Following preincubation with RosetteSep, apheresis product was layered on Ficoll-Paque for density centrifugation at 900 × g for 20 min (no brake). Cells were harvested from the interface and washed with PBS by centrifugation at 500 × g for 5 min and then resuspended in serum (FCS) for cell sorting. All samples were obtained under guidance and approval of the Institutional Review Board of Baylor College of Medicine in accordance with the Declaration of Helsinki. T- and B- cell depleted cultures were incubated with antibodies for CD34 (clone 561, PE conjugate; BioLegend; 1:100) before sorting. The frequency of $CD34^+$ HSC was 0.1–1% following NK cell enrichment (Supplemental Figure 1B). FACS sorting was performed using a BD Aria II cytometer with an 85 µm nozzle at 45 p.s.i. Purity after sorting was >90% (Supplemental Figure 1C). Primary NK cells for short-term imaging were similarly isolated with NK cell RosetteSep.

For FACS analysis of $CD34^+$ intermediates, a six-color flow cytometry panel was performed on a BD Fortessa using antibodies for CD56 (Clone HCD56, Brilliant Violet 605; BioLegend; 1:200), CD3 (Clone UCHT1, Brilliant Violet 711; BioLegend; 1:200), CD16 (Clone 3G8, PE-CF594 conjugate; BD; 1:300), CD94 (Clone DX22, APC conjugate; BioLegend; 1:100), CD117 (Clone 104D2, PE/Cy7 conjugate; BioLegend; 1:10), and CD34 (clone 561, PE conjugate;

BioLegend; 1:100). Flow cytometry data analysis was performed with FlowJo X (TreeStar).

Live-cell imaging and tracking

Cells were imaged in 96-well ImageLock plates (Essen Bioscience) on the IncuCyte ZOOM Live-Cell Analysis System (Essen Bioscience) at 37°C every 2 min in the phase-contrast mode (10× objective). Images were acquired continuously for a 21-d period. NK cell lines and primary NK cells were labeled using CellTracker Violet (Thermo Fisher) at a working concentration of 15 μM and washed with complete media by centrifugation at 500 × *g* for 5 min. Fluorescence images were imported into Imaris (Bitplane) and tracked using the Spot tracking method with the "Autoregressive Motion Expert" setting and removing tracks below an automatic threshold on "Track Duration," keeping approximately the top 20% longest cell tracks.

For tracking of NK developmental intermediates, cells were seeded at 2×10^3 cells per well on a 96-well ImageLock plate with confluent irradiated EL08.1D2 cells and then imaged at 2-min intervals for a 24-h period. Phase-contrast images were segmented with ilastik software by using the "2-stage Autocontext" method for pixel classification to distinguish NKDI from the background (Tu and Bai, 2010; Sommer *et al.*, 2011). An array of cell positions over time was generated from exported binary segmentation images and imported into Imaris (Bitplane) for tracking analysis. The image set was divided into 24 h periods for tracking. Tracking was done using the Spot tracking method on Imaris with the "Autoregressive Motion" setting. Individual tracks were then verified by eye and corrected manually where necessary by using Imaris to fix broken or overlapping tracks. Tracks that we were unable to manually resolve due to cells leaving the field of view or detaching were excluded from further analyses.

Analysis

Track statistics were calculated using Imaris and exported as comma-separated value files, which were graphed using GraphPad Prism. Mean speed was defined as the per-track average of all instantaneous speeds calculated at each frame. Displacement was defined as the absolute distance between cell position at the beginning and the end of the 24-h period of tracking. The straightness parameter was calculated by dividing the displacement by the total path length for each track, so that straightness values close to 1.0 represent highly directed tracks. The arrest coefficient was defined as the percentage of time that the cell stays in arrest based on a threshold on instantaneous speed of 2 μm/min, or approximately one cell body length per image interval. The SD in speed for each track was calculated as the SD in instantaneous speeds observed for a given track. Rose plots were generated by selecting 30 representative tracks per time series and plotting them in Imaris.

For MSD analysis and classification of migration modes, we developed custom MATLAB scripts based on a previously described method for transient migration behavior analysis (Khorshidi *et al.*, 2011). Calculation of MSD was done using @msdanalyzer, a publicly available MATLAB class for MSD analysis of particle trajectories (Tarantino *et al.*, 2014). To implement the method for transient migratory period analysis, each track was analyzed using a sliding window approach and calculating the MSD corresponding to each window. The MSD data were fitted to a curve to estimate the degree of curvature by performing a linear fit against the log-log of the MSD and finding the slope. The diffusion coefficient of a cell in two dimensions is proportional to the slope of the MSD, so to calculate this we did a simple linear fit against the MSD. For fitting purposes, we considered only the first six points of the MSD, as previously described. Track segments were then classified as directed, constrained, or random migration depending on thresholds on these values, which were set to be the same as those previously described (Khorshidi *et al.*, 2011). The threshold for the diffusion coefficient was set at 4.2 $\mu m^2\ min^{-1}$, calculated based on the typical diameter of an NK cell, with all track segments having a smaller diffusion coefficient classified as constrained migration. On the other hand, all segments with an MSD curvature α above 1.5 were defined as directed migration. All remaining segments after these thresholds were applied were classified as diffusive migration. The frequency of alternations between migration modes was defined on a per-track basis as the number of times a cell switched between either constrained, directed, or random migration.

All MATLAB code associated with this paper along with full documentation is available online on the project repository at https://github.com/barclaylee/Incucyte-analysis-toolbox.

Statistics

Statistical analysis was calculated using Prism 6.0 (GraphPad). Ordinary one-way analysis of variance (ANOVA) was used to compare track statistics. Outliers were removed from exported track statistics using the ROUT method in Prism with Q = 1%. For all tests $p < 0.05$ was considered significant.

Sample sizes

Given the various numbers of tracks that met quality thresholds, the sample numbers were not equal for all samples tested. Specifically, the *n* for each representative experiment shown in the figures are as follows: Figure 1B: 75 (NK92), 205 (YTS), 250 (eNK); Figures 2B, 3A, 4A, 5, A and B: 932 (0D), 803 (7D), 134 (14D), 148 (21D); Figures 2C, 3B, and 5C: 607 (0D), 1052 (1D), 699 (2D), 419 (3D), 350 (4D), 372 (5D), 421 (6D), 376 (7D), 725 (8D), 903 (9D), 1022 (10D), 871 (11D), 712 (12D), 291 (13D); Figure 4C: 932; and Figure 4D: 148.

ACKNOWLEDGMENTS

We thank Alexandre Carisey for assistance with coding and useful scientific discussion and Michael Diehl for critical reading of the manuscript. EL08.1D2 stromal cells were a kind gift from Jeffrey Miller and Elaine Dzierzak. This work was supported by the Virginia and L.E. Simmons Family Foundation and an American Society of Hematology Junior Faculty Scholar Award to E.M.M.

REFERENCES

Chan A, Hong DL, Atzberger A, Kollnberger S, Filer AD, Buckley CD, McMichael A, Enver T, Bowness P (2007). CD56bright human NK cells differentiate into CD56dim cells: role of contact with peripheral fibroblasts. J Immunol 179, 89–94.

Choi PJ, Mitchison TJ (2013). Imaging burst kinetics and spatial coordination during serial killing by single natural killer cells. Proc Natl Acad Sci USA 110, 6488–6493.

Coutu DL, Schroeder T (2013). Probing cellular processes by long-term live imaging—historic problems and current solutions. J Cell Sci 126, 3805–3815.

Dezell SA, Ahn YO, Spanholtz J, Wang H, Weeres M, Jackson S, Cooley S, Dolstra H, Miller JS, Verneris MR (2012). Natural killer cell differentiation from hematopoietic stem cells: a comparative analysis of heparin- and stromal cell-supported methods. Biol Blood Marrow Transplant 18, 536–545.

Edsparr K, Johansson BR, Goldfarb RH, Basse PH, Nannmark U, Speetjens FM, Kuppen PJ, Lennernas B, Albertsson P (2009). Human NK cell lines migrate differentially in vitro related to matrix interaction and MMP expression. Immunol Cell Biol 87, 489–495.

Ehrlich LI, Oh DY, Weissman IL, Lewis RS (2009). Differential contribution of chemotaxis and substrate restriction to segregation of immature and mature thymocytes. Immunity 31, 986–998.

Eissens DN, Spanholtz J, van der Meer A, van Cranenbroek B, Dolstra H, Kwekkeboom J, Preijers FW, Joosten I (2012). Defining early human NK cell developmental stages in primary and secondary lymphoid tissues. PLoS One 7, e30930.
Forslund E, Sohlberg E, Enqvist M, Olofsson PE, Malmberg KJ, Onfelt B (2015). Microchip-based single-cell imaging reveals that CD56dimCD57-KIR-NKG2A+ NK cells have more dynamic migration associated with increased target Cell conjugation and probability of killing compared to CD56dimCD57-KIR-NKG2A-NK cells. J Immunol 195, 3374–3381.
Freud AG, Becknell B, Roychowdhury S, Mao HC, Ferketich AK, Nuovo GJ, Hughes TL, Marburger TB, Sung J, Baiocchi RA, *et al.* (2005). A human CD34(+) subset resides in lymph nodes and differentiates into CD56bright natural killer cells. Immunity 22, 295–304.
Freud AG, Yokohama A, Becknell B, Lee MT, Mao HC, Ferketich AK, Caligiuri MA (2006). Evidence for discrete stages of human natural killer cell differentiation in vivo. J Exp Med 203, 1033–1043.
Gerard A, Patino-Lopez G, Beemiller P, Nambiar R, Ben-Aissa K, Liu Y, Totah FJ, Tyska MJ, Shaw S, Krummel MF (2014). Detection of rare antigen-presenting cells through T cell-intrinsic meandering motility, mediated by Myo1g. Cell 158, 492–505.
Grzywacz B, Kataria N, Sikora M, Ooostendorp RA, Dzierzak EA, Blazar BR, Miller JS, Verneris MR (2006). Coordinated acquisition of inhibitory and activating receptors and functional properties by developing human natural killer cells. Blood 108, 3824–3833.
Halkias J, Melichar HJ, Taylor KT, Ross JO, Yen B, Cooper SB, Winoto A, Robey EA (2013). Opposing chemokine gradients control human thymocyte migration in situ. J Clin Invest 123, 2131–2142.
Harris TH, Banigan EJ, Christian DA, Konradt C, Tait Wojno ED, Norose K, Wilson EH, John B, Weninger W, Luster AD, *et al.* (2012). Generalized Levy walks and the role of chemokines in migration of effector CD8+ T cells. Nature 486, 545–548.
Hilsenbeck O, Schwarzfischer M, Skylaki S, Schauberger B, Hoppe PS, Loeffler D, Kokkaliaris KD, Hastreiter S, Skylaki E, Filipczyk A, *et al.* (2016). Software tools for single-cell tracking and quantification of cellular and molecular properties. Nat Biotechnol 34, 703–706.
Huntington ND, Legrand N, Alves NL, Jaron B, Weijer K, Plet A, Corcuff E, Mortier E, Jacques Y, Spits H, Di Santo JP (2009). IL-15 trans-presentation promotes human NK cell development and differentiation in vivo. J Exp Med 206, 25–34.
Khorshidi MA, Vanherberghen B, Kowalewski JM, Garrod KR, Lindstrom S, Andersson-Svahn H, Brismar H, Cahalan MD, Onfelt B (2011). Analysis of transient migration behavior of natural killer cells imaged in situ and in vitro. Integr Biol (Camb) 3, 770–778.
Krummel MF, Bartumeus F, Gerard A (2016). T cell migration, search strategies and mechanisms. Nat Rev Immunol 16, 193–201.
Mace EM, Gunesch JT, Dixon A, Orange JS (2016). Human NK cell development requires CD56-mediated motility and formation of the developmental synapse. Nat Commun 7, 12171.
Miller JS, McCullar V (2001). Human natural killer cells with polyclonal lectin and immunoglobulinlike receptors develop from single hematopoietic stem cells with preferential expression of NKG2A and KIR2DL2/L3/S2. Blood 98, 705–713.
Miller MJ, Wei SH, Parker I, Cahalan MD (2002). Two-photon imaging of lymphocyte motility and antigen response in intact lymph node. Science 296, 1869–1873.
Olofsson PE, Forslund E, Vanherberghen B, Chechet K, Mickelin O, Ahlin AR, Everhorn T, Onfelt B (2014). Distinct migration and contact dynamics of resting and IL-2-activated human natural killer cells. Front Immunol 5, 80.
Rezvani K, Rouce RH (2015). The Application of natural killer cell immunotherapy for the treatment of cancer. Front Immunol 6.
Sommer C, Straehle C, Köthe U, Hamprecht FA (2011). Ilastik: interactive learning and segmentation toolkit. IEEE Int Symp Biomed Imaging: From Nano to Macro, 230–233.
Tarantino N, Tinevez JY, Crowell EF, Boisson B, Henriques R, Mhlanga M, Agou F, Israel A, Laplantine E (2014). TNF and IL-1 exhibit distinct ubiquitin requirements for inducing NEMO-IKK supramolecular structures. J Cell Biol 204, 231–245.
Tu Z, Bai X (2010). Auto-context and its application to high-level vision tasks and 3D brain image segmentation. IEEE Trans Pattern Anal Mach Intell 32, 1744–1757.
Xing F, Yang L (2016). Robust nucleus/cell detection and segmentation in digital pathology and microscopy images: a comprehensive review. IEEE Rev Biomed Eng 9, 234–263.
Yu J, Freud AG, Caligiuri MA (2013). Location and cellular stages of natural killer cell development. Trends Immunol 34, 573–582.
Zhou X, Zhao R, Schwarz K, Mangeat M, Schwarz EC, Hamed M, Bogeski I, Helms V, Rieger H, Qu B (2017). Bystander cells enhance NK cytotoxic efficiency by reducing search time. Sci Rep 7, 44357.